Polymer 50 (2009) 236–244

Contents lists available at ScienceDirect

Polymer

journal homepage: www.elsevier.com/locate/polymer

Sorption and transport of methanol in poly(ethylene terephthalate)

Preeti Chandra, William J. Koros*

School of Chemical and Biomolecular Engineering, Georgia Institute of Technology, Atlanta, GA 30332, USA

ARTICLE INFO

Article history:
Received 11 August 2008
Received in revised form
22 October 2008
Accepted 23 October 2008
Available online 30 October 2008

Keywords:
Sorption
Diffusion
Methanol

ABSTRACT

This paper reports the sorption and diffusion characteristics of methanol vapor in polyethylene terephthalate (PET). Amorphous PET, semicrystalline, biaxially oriented annealed and non-annealed samples have been studied for equilibrium sorption and kinetics of methanol. At activities of methanol less than 0.30, uptake shows Fickian kinetics and isotherm follows the Dual Mode model. Diffusion coefficients increase with penetrant concentration and are of the order of 10^{-10} cm^2/s. Hysteresis during desorption and increase in solubility during resorption suggest methanol induced conditioning effects which may have detrimental effects on the barrier efficacy of PET. At activities greater than 0.30, swelling and relaxation effects occur and the isotherms show Flory–Huggins behavior for all three samples. Uptake follows two-stage kinetics fit by the Berens–Hopfenberg model. Greater polymer chain stability due to annealing reduces the extent of relaxation and improves the barrier efficacy over amorphous and non-annealed, oriented PET. For amorphous PET, at 80% activity and above, an induction time is observed which is absent in the semicrystalline films, suggesting strong relaxation effects in the amorphous phase of PET.

1. Introduction

Poly(ethylene terephthalate) (PET) is a well known barrier material used for packaging of food and beverages, especially carbonated beverages. Growth in the packaged foods and beverages market has led to growth in the market for PET as well. Packaged juices, dairy and beer are some applications with a high growth potential. In most of these instances, retention of taste imparted by the flavor molecules is of primary importance. The flavor is lost either due to flavor scalping or chemical degradation. To estimate the extent of flavor scalping, knowledge of the transport properties of the species is essential. However, measurement of the transport properties of flavor molecules, which are large organic compounds, is difficult due to the low diffusivities which translate into very long experiment times [1]. As a result, actual flavor molecules are much less studied. The interaction of smaller organic species with a polymer can, however, provide insights applicable to such larger molecules over more convenient time scales. For instance, the solubility and diffusivity of a series of organic molecules such as linear and branched alkanes (n-butane, i-butane, n-pentane and i-pentane), linear and branched ketones (acetone, methyl ethyl ketone, methyl isopropyl ketone and methyl n-propyl ketone), linear esters (ethyl acetate and methyl acetate), acetaldehyde, benzene and toluene have been reported at different penetrant activities in biaxially oriented, semicrystalline PET. Solubility and diffusivity of liquid methanol, acetone, dimethyl formamide, dioxane and methylene chloride have also been studied [1–7].

This work studies the transport properties of pure methanol vapor at different activities in an amorphous and two semicrystalline, biaxially oriented samples - one of which is heat set and other which is not. Interaction of PET with methanol is studied and comparison across the samples provides an understanding of the effect of annealing and crystallization on the transport properties of the penetrant.

2. Experimental

2.1. Materials and equipment

Amorphous unoriented, semicrystalline biaxially oriented and semicrystalline biaxially oriented heat-set samples were provided by Coca Cola Company for this work. Methanol of 99.9% purity, ACS grade was purchased from Sigma–Aldrich for the sorption experiments. The film thickness was measured using a micrometer (Ames, Waltham, MA, Model # 56212). The density of the films was obtained using a density gradient column (Techne™, Burlington, NJ) filled with calcium nitrate–water solution. Crystallinity was calculated using wide angle X-ray diffraction studies which were performed on a Rigaku Micro Max 002 system. Cu Kα X-ray source with Ni filter was used. Glass transition temperature was measured using dynamic mechanical analysis performed on a RSA-III

* Corresponding author. Tel.: +1 404 385 2845; fax: +1 404 385 2683.
E-mail address: wkoros@chbe.gatech.edu (W.J. Koros).

0032-3861/$ – see front matter © 2008 Published by Elsevier Ltd.
doi:10.1016/j.polymer.2008.10.031

(Rheometric Instruments), at a scan rate of 2 °C/min and a frequency of 1 Hz, with the temperature starting from room temperature (25 °C) up to a maximum of 200 °C.

2.2. Gravimetric vapor sorption

For vapor sorption at sub-atmospheric pressures, the McBain quartz spring method has been used [8]. This is a gravimetric technique which involves measurement of mass of the sample using a quartz spring as it absorbs the penetrant. The sample is hung on a calibrated quartz spring (GE Sensing, Houston, TX) which can take a maximum load of 50 mg with a maximum extension of 200 mm. The spring and the sample are placed in a glass chamber maintained at 35 °C by a hot water jacket. The rest of the manifold is also heated to prevent condensation of the vapor on the side walls. The sample position is determined by focusing on a crosshair on the spring using a precision cathetometer. Together, the cathetometer and the 50–200 spring provide a measurement accuracy of 1.25 μg. The entire system had a leak rate of less than 2 torr/week.

The sample is loaded and evacuated overnight before sorption is started. During evacuation, a liquid nitrogen trap is used. Prior to the introduction of the vapor at a given pressure into the sample chamber, all air in the headspace of the liquid vial and dissolved gases are removed by five freeze–pump–thaw cycles. Sorption kinetics are obtained by recording the spring position at different times after introduction of the vapor. Equilibrium is assumed to be attained when the spring position does not change over the course of 24 h. Once equilibrium is reached, the pressure is increased by introducing more vapor during sorption. The concentration of methanol in the polymer (C, ccSTP/ccpoly) is calculated using Eq. (1)

$$C = \left(\frac{K\Delta x}{g}\right)\frac{22,414 \times \rho_p}{M_W \times M_p} \quad (1)$$

K (g/s^2) is the calibration constant of the spring, g (cm/s^2) is the rate of acceleration due to gravity, Δx (cm) is the change in spring position, ρ_p (g/cc) is the polymer density, M_p (g) is the mass of the polymer sample hung on the spring, M_W(=32 g/mol) is the molecular weight of methanol. Desorption of methanol was performed by reducing its partial pressure to the desired value by evacuation.

3. Results and discussion

3.1. Polymer characterization

Table 1 shows the properties of the films. The crystalline weight fraction was calculated from the sample density (ρ) using the two-phase model represented in Eq. (2). The amorphous phase density (ρ_a) is taken to be 1.331 g/cc and the density of PET crystals (ρ_c) is taken to be 1.455 g/cc [9]. It must be noted here that there is not complete agreement in literature over the density of the ideal crystalline phase. Apart from 1.455 g/cc reported by Daubeny [10], Fakirov and coworkers calculated the density to be 1.515 g/cc for many samples annealed between 120 °C and 260 °C and 1.484 g/cc for one sample annealed at 100 °C [11]. Based on the ideal crystal density used for calculation, the estimated crystallinity of the films can vary substantially. It was found that the value of 1.455 g/cc is a well accepted value [9,12]. Therefore, this value has been used for this work.

$$X_c = \left(\frac{\rho - \rho_a}{\rho_c - \rho_a}\right)\frac{\rho_c}{\rho} \quad (2)$$

Table 1
Physical properties of the polymer samples.

Sample	Thickness (micron)	T_g (°C)	Density (g/cc)	Crystallinity from density (w/w%)	Crystallinity from WAXD (w/w%)
Amorphous	29.2 ± 1.3	85	1.3339	3	0.00
Semicrystalline annealed	18.6 ± 1.0	115	1.3872	48	39
Semicrystalline non-annealed	15.2 ± 1.0	116	1.3844	45	39

Crystalline fraction from X-ray diffraction pattern has been calculated by taking the ratio of the area of the crystalline peaks with respect to the total peak area. Results are shown in Table 1. As may be noted, the crystallinity estimate from density and XRD characterization is different for the semicrystalline samples. Varying estimates of crystallinity, obtained from different methods such as DSC, density, infrared spectroscopy and XRD, is very common in the polyester characterization literature. Ward and Farrow [13] obtained X_c based on XRD, density and IR, and found them to be consistently different. Based on the characterization of a large number of samples with varying crystallinity and orientation, Abhiraman and coworkers [14] concluded that none of these techniques, which measure fundamentally different physical properties, give identical phase estimations. Liu et al. [15] also found that crystallinity determinations from DSC, IR and density do not match and attribute differences to dependence on heat of fusion and crystal phase density. Many researchers have reconciled these differences by combining results from say, density, XRD and IR, to obtain the density of the third phase [13,16–18]. However, given the fundamentally different measurements from each method and the need to use other data such as crystal phase density or the heat of fusion, these three phase estimations also have uncertainty. Considering its simplicity and applicability, the two-phase model has been used for sorption characterization in this work, and the crystalline weight fractions estimated from XRD have been used in later sections. X-ray diffraction has the advantage of being independent of physical properties such as crystal phase density. The estimated crystalline fraction is thus, likely to be more accurate. As will be shown in subsequent sections, the two-phase model with crystallinity from XRD measurement has been found to correlate well with measured transport properties. Glass transition temperatures are also shown in Table 1.

3.2. Equilibrium sorption

Sorption experiments at low activities were performed in small steps of increasing pressure to investigate the dual mode characteristics. At higher activities, larger increments of activity were applied. The isotherms obtained in the low activity range are shown in Fig. 1. In this activity range, the isotherms show distinct concavity to the x-axis (fugacity or activity). This is commonly observed for glassy polymers and is described by the Dual Mode Model. According to this model, sorption of a penetrant in a polymer may be described by Eq. (3), [2,19,20]. The first term represents Langmuir type sorption in the non-equilibrium regions or 'holes' of the glassy polymer and the second term represents Henry's Law sorption in the equilibrium or 'dissolved' regions.

$$C = \frac{C'_H bp}{(1 + bp)} + k_d p \quad (3)$$

C'_H is the saturation capacity of these holes, b is the affinity constant, and p is the pressure of the penetrant outside the polymer, and k_d is Henry's Law solubility constant. As shown in Fig. 1, dual mode behavior, i.e. concavity of the isotherm to the x-axis, was evident until $p/p_o \approx 0.25$ in all the three samples. The last point on each isotherm is plotted to show the activity at which deviation from

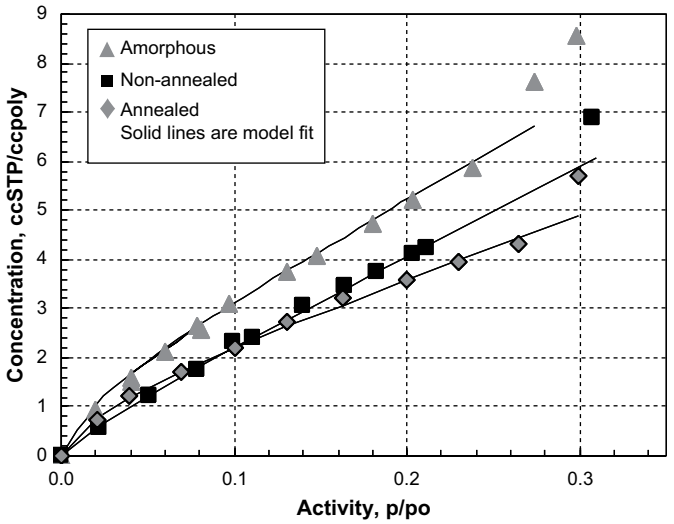

Fig. 1. Sorption isotherm at low activities of methanol indicating the dual mode characteristics. Solid lines correspond to Dual Mode Model fit. The last points at 30% activity show the initiation of positive deviation from dual mode behavior at intermediate activities.

dual mode occurs. The solid lines are the dual mode model fit of Eq. (3). Parameters C'_H, b and k_d obtained are shown in Table 2. As can be seen, the affinity constant, b, is the same within experimental uncertainty for all the three samples. This is to be expected because the affinity constant is primarily representative of the polymer–penetrant interaction. These values are at the same order of magnitude as that of other small interacting penetrants such as ethyl acetate, benzene and acetone already studied in literature [1–3]. Morphological differences between the samples are not expected to change the molecular level interaction of the penetrant with the polymer chains. However, Henry's Law solubility constant, k_d, and the Langmuir saturation capacity, C'_H, will be affected by morphological changes because these are dependent on the number of sorption sites available in the polymer, which in turn will depend on the fraction and morphology of the amorphous phase. According on the two-phase model, these values should be proportional to the crystallinity. For the semicrystalline samples, Eq. (3) then becomes

$$C = \frac{\phi_a C'_H bp}{(1+bp)} + \phi_a k_d p \tag{4}$$

where ϕ_a is the amorphous volume fraction, and the dual mode model parameters are those evaluated for a completely amorphous sample. Based on the crystallinity levels determined by X-ray diffraction, the estimated values for C'_H and k_d are shown in Table 3. The actual k_d for the annealed sample is within the error of the prediction. Post-biaxial orientation, this sample has been annealed at 210 °C which is higher than the typical crystallization temperature of 150 °C, is high enough to allow substantial rearrangement of the oriented, non-crystalline regions [21]. The close match between the predicted and the actual k_d of the amorphous region of this sample suggests that the morphology of the

Table 2
Dual mode model parameters for methanol.

Parameter	Amorphous	Annealed, semicrystalline	Non-annealed, semicrystalline
b (atm^{-1})	134 ± 35	124 ± 28	144 ± 15
C'_H (ccSTP/ccpoly)	1.37 ± 0.07	1.22 ± 0.06	0.7 ± 0.1
k_d (ccSTP/ccpoly/atm)	74 ± 5	48 ± 7	63 ± 2

Table 3
Dual mode model parameters predicted by the two-phase model.

Parameter	Annealed, semicrystalline	Non-annealed, semicrystalline
$\phi_a C'_{H,amorphous}$ (ccSTP/ccpoly)	0.88 ± 0.06	0.88 ± 0.11
$\phi_a k_{d,amorphous}$ (ccSTP/ccpoly/atm)	47 ± 7	47 ± 2

polymer segments in 'Henry's Law region' of the amorphous phase is similar to that of the completely amorphous sample. The crystals are well formed after the orientation and annealing process and the two-phase model can closely predict the sorption behavior. On the other hand, the observed C'_H is higher than predicted. C'_H is determined by the non-equilibrium Langmuir sites in the polymer, which in turn will be influenced by the rate of quenching after annealing above the T_g (at which temperature there are no non-equilibrium sites). A very fast quench will create more non-equilibrium sites than a slower quench where segmental mobility is retained for a longer period and allows the chains to come closer to an equilibrium packing. For gases, Micheals and Bixler also observed that the C'_H for an annealed, semicrystalline sample was higher than predicted by the two-phase model based on the amorphous film value [22]. Differences in transport properties between annealed and non-annealed semicrystalline samples, therefore, are to be expected and will not be easily predicted by simple normalization using the two-phase model and amorphous sample.

In the case of the oriented, non-annealed sample, the C'_H is closer to the predicted value. On the other hand, the k_d value is higher than predicted. The factors which determine the final morphology of this sample are its starting morphology, sample history, draw temperature, axial and transverse draw ratios, and the sequence of drawing (i.e. whether drawing in the machine direction and transverse direction was done sequentially or simultaneously) [21]. Comparison of the actual k_d value with the predicted value for the non-annealed sample suggests that biaxial orientation has created more free volume in Henry's Law domains of the amorphous phase of the non-annealed sample relative to the completely amorphous sample. As a result, the actual value is more than the predicted values. Ward and coworkers observed that in the case of simultaneously drawn films with equal draw ratios in both directions and a draw temperature of 80 °C, the oxygen permeability increased with increasing draw ratios and was always higher than prediction based only on amorphous content [23]. With regard to C'_H, apart from strain rate and draw ratio, the drawing temperature becomes crucial. If the draw temperature is above T_g, the C'_H will depend on the quench rate. On the other hand, if the drawing temperature is below T_g, C'_H will depend only on the draw ratio and the strain rate. Not knowing these conditions for the current commercially prepared samples prevents one from reaching definite conclusions regarding the observed and predicted C'_H values. The reader is also referred to published work by Ward and coworkers [24], and Vieth and coworkers [25]. Consistent with our results, these reports suggest that with limited information about sample processing conditions, definite conclusions about the effect of orientation on the number of non-equilibrium sites in the non-annealed, oriented film may not be drawn.

Sorption isotherms of methanol in all the three as-received samples were obtained till a maximum activity of 0.96. Fig. 2 shows the isotherms of the three PET samples at 35 °C. At 30% activity and beyond, the isotherms are clearly convex to the x-axis. Such isotherms have been observed for several polymers, especially for strongly sorbing organic vapors and gases [26,27]. This behavior is well explained by Flory–Huggins sorption theory [28]. The isotherm described by Eq. (5) is also applicable to rubbery polymers which show linearity of concentration with pressure at low uptakes.

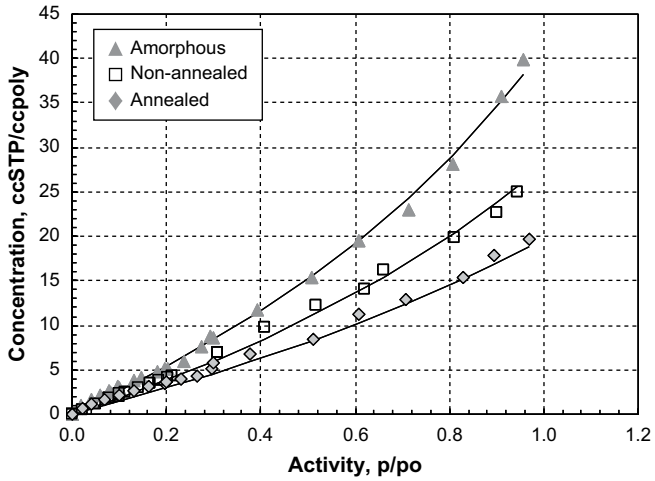

Fig. 2. Methanol sorption isotherm in PET at 35 °C. Solid lines correspond to Flory–Huggins fit. Positive deviation from the Flory–Huggins fit at the low activities is due to dual mode behavior.

$$\ln\left(\frac{p}{p_o}\right) = \ln\phi + (1-\phi) + \chi(1-\phi)^2 \quad (5)$$

In Eq. (5) p is the pressure of the gas/vapor, p_o is the saturation vapor pressure at the temperature of operation, χ is Flory–Huggins interaction parameter, and ϕ is the volume fraction of the penetrant in the polymer. The solid lines in Fig. 2 are obtained by curve fitting the experimental data to Eq. (4) with a constant Flory–Huggins interaction parameter (χ). Table 4 shows the parameter values obtained. Since the crystals of PET are impermeable, and the sorbed molecules reside only in the amorphous regions, the similarity in the value of the interaction parameter for each of the three samples is to be expected.

The total uptake as weight percent at 96% activity by each sample is also shown in Table 4. The amorphous sample swells considerably and absorbs 4.3 wt% methanol which corresponds to a volume fraction of 0.067 in the polymer. This value agrees well with the uptake of 0.06 volume fraction, reported by Durning and Billovits for liquid methanol ($p/p_o = 1$) [6]. However, for the annealed film with 0.631 amorphous volume fraction, the uptake of 2.0 wt% corresponds to only 46.5% of the amorphous PET film, which is lower than the prediction based on the two-phase model. In the non-annealed, oriented film with amorphous volume fraction of 0.626, the uptake is 58.1% of the amorphous PET and matches the two-phase model prediction quite closely. Swelling in the annealed semicrystalline sample is less than expected because the annealing leads to stabilization of the amorphous phase morphology and reduces the free volume, making it more difficult to swell. Zhou and Koros observed increased resistance to swelling and plasticization by acetic acid and water after sub-T_g thermal annealing of Matrimid™ hollow fibers due to decreased free volume and charge transfer complexes [29]. Wind and coworkers observed that annealing stabilized the amorphous polyimide and increased the plasticization pressure in the presence of high pressure CO_2 [30]. Additionally, in a semicrystalline polymer, the restraining effect of the crystals further reduces the chain mobility in the amorphous phase. In the non-annealed, semicrystalline sample, the actual uptake is only slightly less than what is predicted. It is believed that the film extrusion and orientation processes are the same for both samples, the only difference between them is annealing. Therefore, it may be concluded that annealing is the dominant factor, and not the restraining effect of the crystals, that causes a reduction in the swelling of the amorphous regions in this case. Michaels suggested that in most cases, segmental motion in glassy polymers is already too low to be significantly influenced by the crystals. For low levels of swelling the primary effect of crystallinity on sorption is reduction in available amorphous regions into which sorption can occur [31]. Evidence in our work also points to limited influence of the crystal restriction on the amorphous phase swelling of semicrystalline samples. However, it must be noted here that for penetrants with higher solubility than methanol, the amorphous regions may swell more, resulting in increased segmental motion. Under such a situation, if there is a large decrease in the glass transition temperature of the polymer–solvent system, chain immobilization due to crystallinity could become more important. However, in the case of methanol, and other penetrants with similar sorption levels in PET, this effect is less dominant.

Table 4
Flory–Huggins interaction parameter and the mass uptake at $p/p_o = 0.96$ for methanol in PET.

	Amorphous	Annealed, Semicrystalline	Non-annealed, semicrystalline
χ	2.03 ± 0.01	2.57 ± 0.02	2.33 ± 0.01
Uptake at $p/p_o = 0.96$ (g/100 g poly)	4.3	2.0	2.5

While swelling effects are evident only at high activities of methanol, at lower activities in the dual mode model region, history dependent conditioning of the polymer matrix occurs. Upon desorption of methanol from a sample exposed to a maximum of $p/p_o = 0.30$, hysteresis was observed, which is indicative of the conditioning effect of methanol. All the three samples show this effect. The hysteresis is largest in the amorphous film and lowest in the annealed, oriented film. This result is due to the annealing process which reduces the free volume and improves the chain packing, which therefore enhances the resistance to conditioning effects and is consistent with the lower swelling effects. The amorphous and the non-annealed films have not gone through such a thermal stabilization step and show much greater susceptibility to conditioning. Koros and Paul observed hysteresis in desorption isotherms of CO_2 in PET after exposure to CO_2 at 20 atm [32]. Similar effects have been observed in the polycarbonate–CO_2 system as well [33,34]. Berens observed hysteresis during desorption of vinyl chloride from poly(vinyl chloride). The hysteresis was larger in samples exposed to higher activities of the vapor [35]. This conditioning effect becomes important for barrier materials because a conditioning penetrant can lead to increased gas permeability during multi-component permeation and loss of

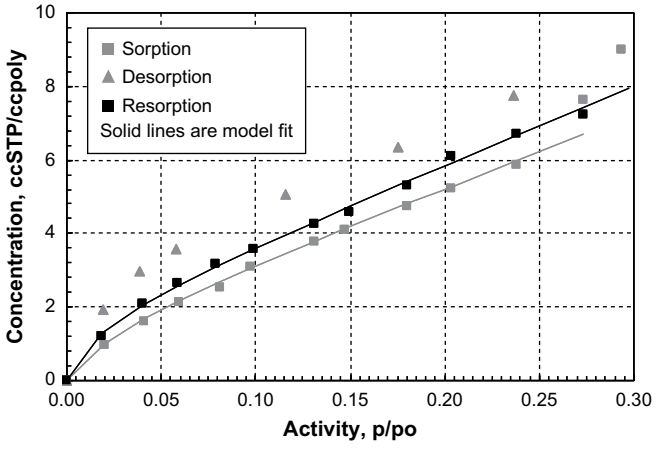

Fig. 3. Resorption isotherm of methanol in amorphous PET. The first sorption and desorption isotherms are shown for reference.

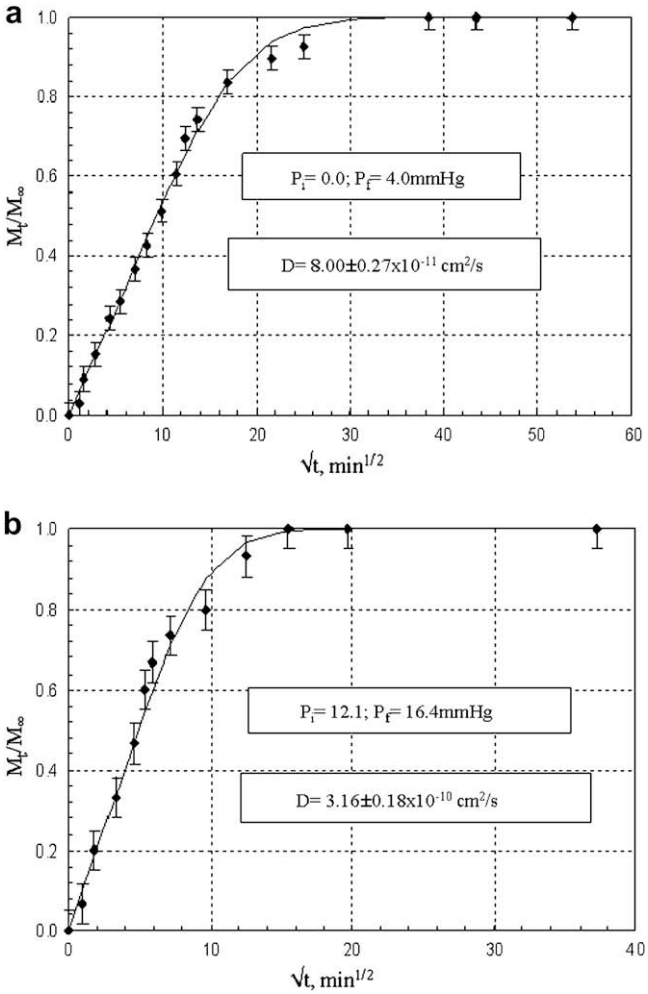

Fig. 4. Fickian kinetics of methanol vapor in amorphous PET (a) $P_i = 0.0$ mmHg, $P_f = 4.0$ mmHg, $D = 8.00 \pm 0.27 \times 10^{-11}$ cm^2/s; (b) $P_i = 12.1$ mmHg, $P_f = 16.4$ mmHg, $D = 3.16 \pm 0.18 \times 10^{-10}$ cm^2/s.

barrier efficacy due to an increase in the free volume of the system. Many literature reports confirm an increase in free volume through resorption in conditioned polymers [34,36,37]. Connelly et al. found that pre-swelling of PMMA with organic molecules such as methanol led to a higher initial solubility of water, methanol, and ethanol at low pressures [38]. Similarly, in PET, sorption of low pressure acetaldehyde increased by a factor of 3.5 after exposure to high activity vapor [39]. Increased and faster propane sorption was observed in polystyrene microspheres pre-swollen with propane [40]. As is shown in Fig. 3, increased solubility and hence, increase in free volume is apparent upon performing resorption of methanol in amorphous PET that was exposed to methanol vapor at 0.28 activity followed by complete desorption.

3.3. Sorption kinetics

Sorption kinetics of methanol at various activities were obtained using interval sorption to estimate the diffusion coefficient and to assess the mode of transport (Fickian vs. non-Fickian). At low activities, with small increases in the methanol pressure, Fickian kinetics were observed. Eq. (6) below represents mass uptake governed by Fick's Law for a film of thickness 2*l*.

$$\frac{M_t}{M_\infty} = 1 - \frac{8}{\pi^2}\sum_{n=0}^{\infty}\frac{1}{(2n+1)^2}\exp\left[-\frac{(2n+1)^2\pi^2 Dt}{4l^2}\right] \quad (6)$$

M_t is the mass uptake/removal at time t, M_∞ is the amount absorbed/desorbed at equilibrium, D is the diffusivity. Diffusion coefficients were calculated by curve fitting the experimental data to Eq. (6). Not surprisingly, given the interaction effects between the polymer and the penetrant, concentration dependent diffusion coefficients were obtained. A few representative kinetics that were obtained for the amorphous, non-annealed and annealed PET films, are shown in Figs. 4–6 respectively. The kinetics show Fickian characteristics [41] up to $p/p_o = 0.20$ in the amorphous film, $p/p_o = 0.24$ in the non-annealed, oriented film, and $p/p_o = 0.30$ in the annealed film. Thereafter, some long term glassy state relaxation effects are visible in the sorption kinetics. It was observed that the diffusion coefficients increase with concentration of the penetrant in the polymer. This was also confirmed by performing desorption experiments which showed that desorption was slower than sorption [42] Diffusion coefficients in the activity range where the Fickian kinetics are exhibited are plotted with respect to activity in Fig. 7. For diffusion, the dual mode model also predicts effective diffusion coefficients which increase with increasing concentration to reach an asymptotic value [9]. Fig. 7 suggests that the concentration dependence observed here could be due to the difference in the diffusion coefficients in the two sorption domains - the 'holes' and the 'dissolved' regions. At low concentrations, dissolution is favored in the 'holes', which results in a low diffusivity. As concentration increases, both diffusivity and the fraction of molecules in the equilibrium region increase. The solid lines in Fig. 7 show the dual mode model fit using Eq. (7) below.

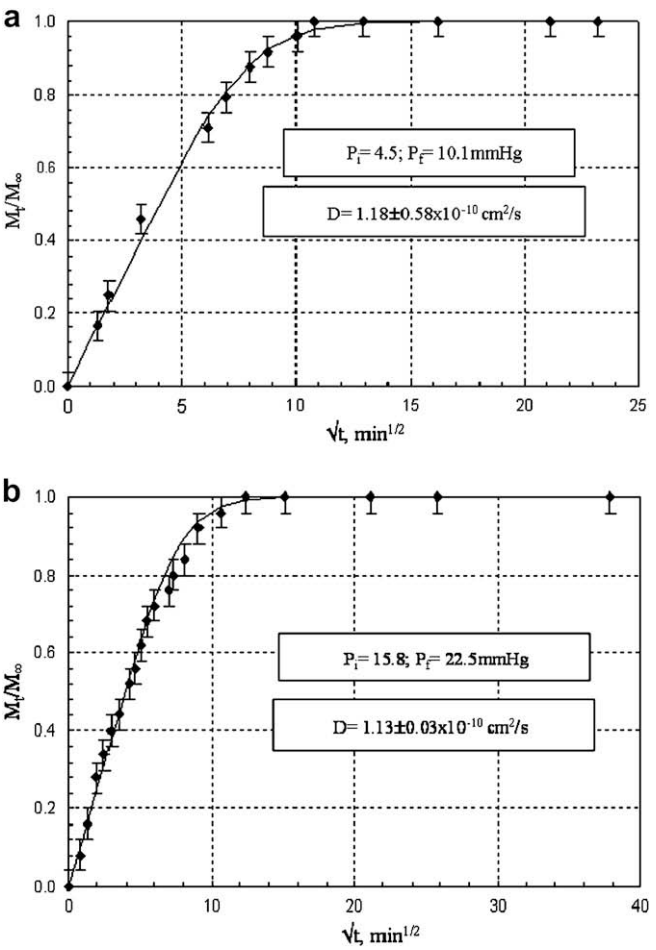

Fig. 5. Fickian kinetics of methanol vapor in non-annealed PET (a) $P_i = 4.5$ mmHg, $P_f = 10.1$ mmHg, $D = 1.18 \pm 0.58 \times 10^{-10}$ cm^2/s; (b) $P_i = 10.1$ mmHg, $P_f = 15.8$ mmHg, $D = 1.26 \pm 0.03 \times 10^{-10}$ cm^2/s.

$$D_{\mathrm{eff}} = D_{\mathrm{D}}\left[\frac{\left(1+FK/(1+\alpha C_{\mathrm{D}})^2\right)}{\left(1+K/(1+\alpha C_{\mathrm{D}})^2\right)}\right] \tag{7}$$

$$C_{\mathrm{D}} = k_{\mathrm{D}}\cdot p \tag{8}$$

$$F = \frac{D_{\mathrm{H}}}{D_{\mathrm{D}}} \tag{9}$$

$$K = \frac{C_{\mathrm{H}}' b}{k_{\mathrm{D}}} \tag{10}$$

$$\alpha = b/k_{\mathrm{D}} \tag{11}$$

D_{eff} is the effective local diffusion coefficient. C_{D} is the concentration of the penetrant in the dissolved regions (Henry's Law domains), D_{D} is the diffusion coefficient for penetrant jumps from one Henry's law site to another, D_{H} is the diffusion coefficient primarily for penetrant jumps from a 'hole' to a Henry's Law site and F, K and α are as defined by Eqs. (7)–(11) respectively.

Table 5 shows the values of F obtained from the curve fit. The ratio $F = D_{\mathrm{D}}/D_{\mathrm{H}}$ is very small in each case ($\sim$0.004), and can be assumed to be negligible. This implies that methanol is practically immobilized in the non-equilibrium sites. Upon comparison of with the values of F for CO_2 and O_2 with that of methanol, it is observed that by increasing penetrant size and critical temperature, F decreases. Critical temperature is a measure of the condensability of the molecule. By increasing condensability, the non-equilibrium sites become energetically more favorable for accommodation of sorbed penetrant, and it is difficult for the molecule to jump out into the dissolved region. The diffusivity in the equilibrium domains, D_{D}, and the infinite dilution diffusion coefficient are shown in Table 6. The infinite dilution diffusivity is evaluated using Eq. (7) at $p \to 0$ or $C_{\mathrm{D}} \to 0$.

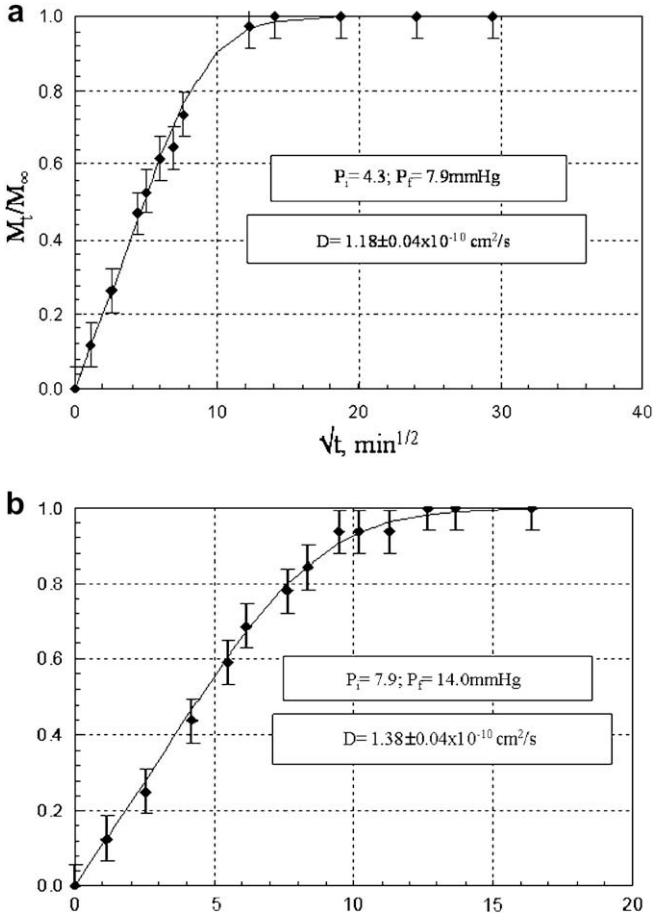

Fig. 6. Fickian kinetics of methanol vapor in annealed PET (a) $P_i = 4.3$ mmHg, $P_f = 7.9$ mmHg, $D = 1.18 \pm 0.04 \times 10^{-10}$ cm^2/s; (b) $P_i = 7.9$ mmHg, $P_f = 14.0$ mmHg, $D = 1.38 \pm 0.04 \times 10^{-10}$ cm^2/s.

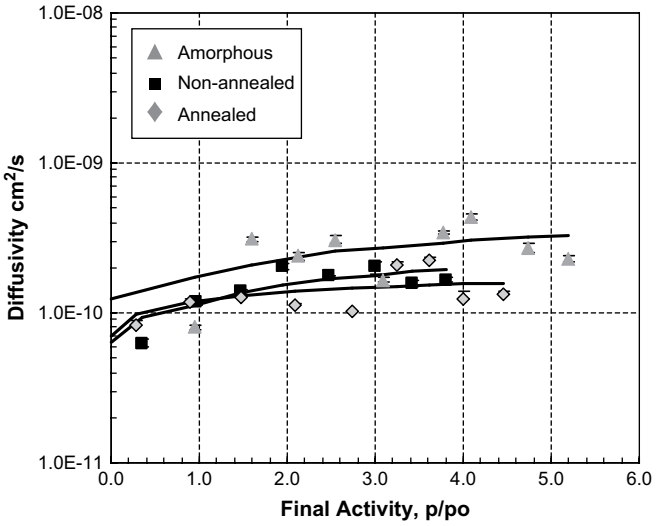

Fig. 7. Diffusivity of different PET samples, obtained at different activities. Solid lines are the fit of the dual mode model for diffusion coefficient (Eq. (4)).

Sorption kinetics were obtained at activities greater than 0.25 on all samples as well. At these intermediate and high activities, the sorption kinetics were non-Fickian and significant long term relaxation effects were observed. Interacting penetrants at high activities, such as benzene, acetone, dimethyl formamide, methylene dichloride, acetaldehyde, methyl ethyl ketone and methyl acetate has also shown non-Fickian kinetics in PET [1,2,5,6,43]. Kinetics obtained at intermediate activities of $p/p_o = 0.40$ and $p/p_o = 0.50$ have been shown in Figs. 8 and 9. These are typical two-stage kinetics where the initial Fickian uptake is followed relaxation. The first stage, which occurs at small times, is diffusion controlled, and the uptake is linear with the square root of time. The second stage, at long times, is a relaxation controlled regime. The second stage persists for a long time and pertains to the slow polymer chain relaxations. Berens and Hopfenberg proposed a parallel model for two-stage sorption that allowed separation of the relaxation and diffusion parameters [44]. Eqs. (12)–(15) represent the Berens–Hopfenberg Model. The total uptake (M_t) at any time t can be written as

$$M_t = M_{t,\mathrm{R}} + M_{t,\mathrm{F}} \tag{12}$$

$M_{t,\mathrm{R}}$ and $M_{t,\mathrm{F}}$ are the amounts absorbed due to relaxation (subscript R) and Fickian diffusion (subscript F) respectively. $M_{\infty,\mathrm{F}}$ is the equilibrium uptake due to Fickian diffusion. The relaxation uptake is assumed to be first order in the driving force, which is the

Table 5
Comparison of the ratio of diffusivities, F, of various molecules.

Gas molecule	Collision diameter (Å)	Critical temperature (K)	$F = D_{\mathrm{D}}/D_{\mathrm{H}}$
O_2 [42]	3.0	154.35	0.140
CO_2 [9]	3.4	304.15	0.078
CH_3OH	4.5	513.15	0.004

Table 6
Methanol diffusivity in the equilibrium regions of PET.

PET sample	D_D (cm^2/s)	Infinite dilution diffusivity (cm^2/s)
Amorphous	$4.21 \pm 0.50 \times 10^{-10}$	1.23×10^{-10}
Annealed, semicrystalline	$2.68 \pm 0.38 \times 10^{-10}$	6.35×10^{-11}
Non-annealed, semicrystalline	$1.83 \pm 0.19 \times 10^{-10}$	8.28×10^{-11}

concentration difference between relaxation uptake at time t ($M_{t,R}$) and the equilibrium uptake due to relaxation ($M_{\infty,R}$). The relaxation rate constant is k_R.

$$M_t = \phi_F\left\{1 - \frac{8}{\pi^2}\sum_{n=0}^{\infty}\frac{1}{(2n+1)^2}\exp\left[-(2n+1)^2 k_F t\right]\right\} + (1-\phi_F)(1-\exp(-k_R t)) \quad (13)$$

$$k_F = \frac{\pi^2 D}{4l^2} \quad (14)$$

$$\phi_F = M_{\infty,F}/M_\infty \quad (15)$$

Eq. (13) indicates that as the penetrant approaches equilibrium, the rate of uptake decreases, and true equilibrium is reached only at $t \to \infty$. Extremely long times are often experimentally inaccessible due to time constraints. Therefore, equilibrium is assumed to be reached once absorption does not increase within the error of measurement, or when the error in measurement will be at the most 1–2%. Thus, the measured M_∞ is 98–99% of the actual equilibrium value. Kinetics shown in Figs. 8 and 9 are fit to Eq. (13). The parameters obtained are mentioned along with the diffusion and relaxation time constants in Table 7. As is the case with two-stage kinetics, the relaxation rate is slower than the diffusion rate. These parameters trend well when compared with those evaluated for other lower alcohols such as ethanol, i-propanol and n-propanol. The authors will follow up with more analysis in subsequent work [42]. It is seen in both figures that the diffusion rate and relaxation rate are slower in the non-annealed, semicrystalline PET film than the amorphous and annealed films. The slower relaxation is contrary to what was observed by Hopfenberg and coworkers in polystyrene-n-pentane. They found that relaxation rate was higher

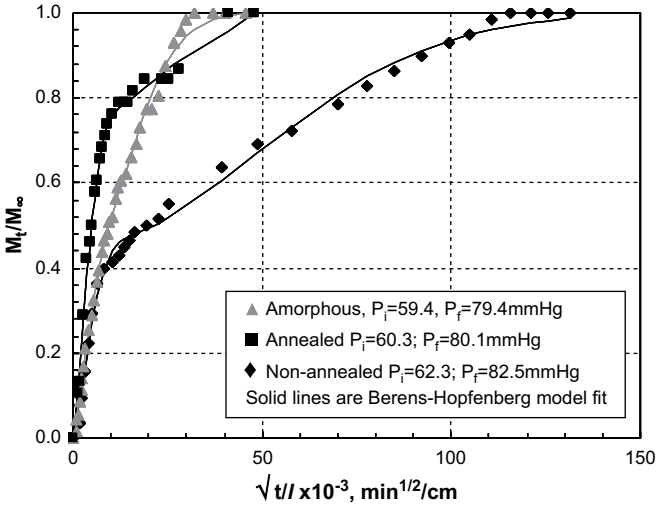

Fig. 8. Sorption kinetics of different PET samples at 35 °C at $p/p_o = 0.40$. Amorphous: $D = 2.64 \pm 0.33 \times 10^{-10}$ cm^2/s, $k_R = 2.13 \pm 0.10 \times 10^{-5}$ s^{-1}, $\phi_F = 0.37 \pm 0.02$; Annealed PET: $D = 2.48 \pm 0.15 \times 10^{-10}$ cm^2/s, $k_R = 2.02 \pm 0.32 \times 10^{-5}$ s^{-1}, $\phi_F = 0.74 \pm 0.01$; Non-annealed PET: $D = 1.84 \pm 0.20 \times 10^{-10}$ cm^2/s, $k_R = 0.62 \pm 0.03 \times 10^{-5}$ s^{-1}, $\phi_F = 0.45 \pm 0.01$.

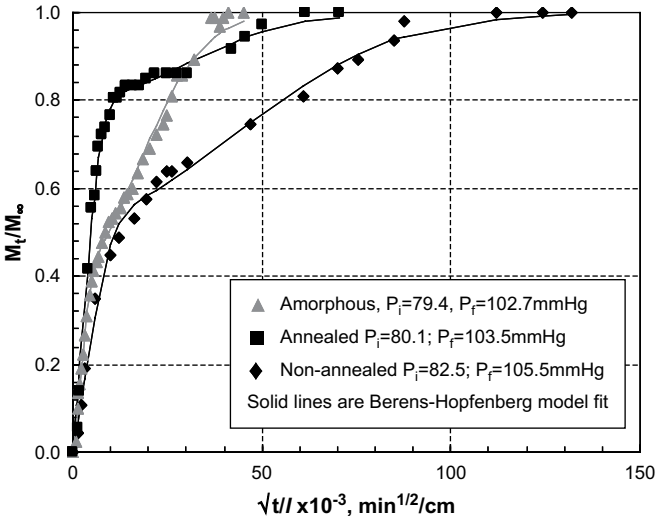

Fig. 9. Sorption kinetics of different PET samples at 35 °C at $p/p_o = 0.50$. Amorphous PET: $D = 4.86 \pm 0.44 \times 10^{-10}$ cm^2/s, $k_R = 1.31 \pm 0.05 \times 10^{-5}$ s^{-1}, $F_F = 0.42 \pm 0.01$; Annealed PET: $D = 2.16 \pm 0.14 \times 10^{-10}$ cm^2/s, $k_R = 1.16 \pm 0.22 \times 10^{-5}$ s^{-1}, $\phi_F = 0.80 \pm 0.01$; Non-annealed PET: $D = 1.15 \pm 0.14 \times 10^{-10}$ cm^2/s, $k_R = 0.80 \pm 0.06 \times 10^{-5}$ s^{-1}, $\phi_F = 0.54 \pm 0.01$.

in the uniaxially oriented glassy films than the annealed samples [45]. Orientation leads to residual stresses in the polymer. Despite the higher final uptake in the non-annealed film relative to the annealed film, the residual stresses seem to slow down the relaxation process in the former sample. It may be concluded that the activation energy of the process is higher. Moreover, due to a greater degree of polymer chain stability in the annealed sample, a larger fraction of the uptake is contributed by Fickian diffusion in the annealed sample than the amorphous and non-annealed samples. Less stress and lower susceptibility to swelling result in lower uptake due to relaxation in the annealed film.

At 80–95% activity, both semicrystalline samples show two-stage kinetics. As at intermediate activities, the non-annealed film relaxes much more slowly than the annealed film. The kinetics are shown in Fig. 10. However, kinetics for amorphous PET, shown in Fig. 11 have some interesting and unusual features. Two things stand out: (a) there is an induction period of nearly 1.0 min in each of the three cases; (b) the sorption shows Fickian characteristics with the diffusivity increasing with activity or concentration. The occurrence of these features together represents a dichotomy.

Table 7
Parameters that define the non-Fickian relaxation kinetics shown in Figs. 8–10 and relative rate of diffusion vs. relaxation.

PET sample	Amorphous	Annealed, semi-crystalline	Non-annealed, semicrystalline
$p/p_o = 0.40$ (with reference to Fig. 8)			
D	$2.64 \pm 0.33 \times 10^{-10}$	$2.48 \pm 0.15 \times 10^{-10}$	$1.84 \pm 0.20 \times 10^{-10}$
k_F	$3.06 \pm 0.38 \times 10^{-4}$	$2.87 \pm 0.17 \times 10^{-4}$	$2.13 \pm 0.23 \times 10^{-4}$
k_R	$2.13 \pm 0.10 \times 10^{-5}$	$2.02 \pm 0.32 \times 10^{-5}$	$0.62 \pm 0.03 \times 10^{-5}$
ϕ_F	0.37 ± 0.02	0.74 ± 0.01	0.45 ± 0.01
$p/p_o = 0.50$ (with reference to Fig. 9)			
D	$4.86 \pm 0.48 \times 10^{-10}$	$2.16 \pm 0.14 \times 10^{-10}$	$1.15 \pm 0.14 \times 10^{-10}$
k_F	$1.39 \pm 0.14 \times 10^{-3}$	$6.16 \pm 0.40 \times 10^{-4}$	$3.28 \pm 0.04 \times 10^{-4}$
k_R	$1.31 \pm 0.05 \times 10^{-5}$	$1.16 \pm 0.22 \times 10^{-5}$	$0.80 \pm 0.06 \times 10^{-5}$
ϕ_F	0.42 ± 0.01	0.80 ± 0.01	0.54 ± 0.01
$p/p_o = 0.95$ (with reference to Fig. 10)			
D		$3.57 \pm 0.53 \times 10^{-10}$	$1.70 \pm 0.24 \times 10^{-10}$
k_F		$1.53 \pm 0.23 \times 10^{-3}$	$7.26 \pm 0.03 \times 10^{-4}$
k_R		$2.05 \pm 0.23 \times 10^{-5}$	$1.15 \pm 0.08 \times 10^{-5}$
ϕ_F		0.52 ± 0.02	0.44 ± 0.02

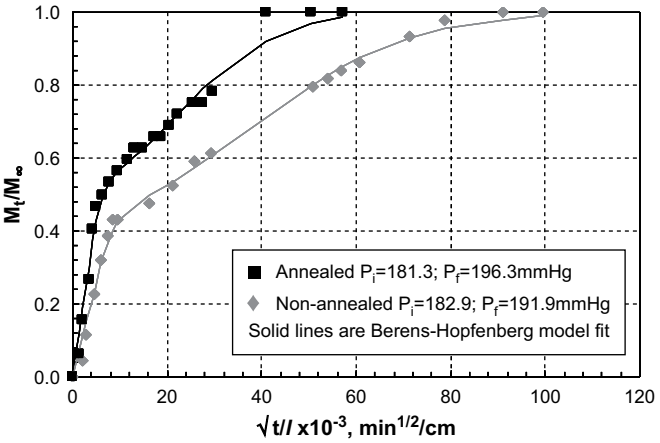

Fig. 10. Kinetics of the semicrystalline samples at $p/p_o = 0.95$ at 35 °C. Annealed PET: $D = 3.57 \pm 0.53 \times 10^{-10}$ cm^2/s, $k_R = 2.05 \pm 0.23 \times 10^{-5}$ s^{-1}, $\phi_F = 0.52 \pm 0.02$; Non-annealed PET: $D = 1.70 \pm 0.24 \times 10^{-10}$ cm^2/s, $k_R = 1.15 \pm 0.08 \times 10^{-5}$ s^{-1}, $\phi_F = 0.44 \pm 0.02$.

It is believed that this induction is statistically significant. A comparison with Fickian kinetics at lower activities in Fig. 4 shows that sorption is measurable after 1 min of vapor introduction. The total mass uptake in these low activity cases is actually less than at the higher activities being considered here. Thus, at small times, the mass change is also correspondingly small. Nevertheless, it is measurable and correlates well with the Fickian prediction. Therefore, it is believed that the induction period observed here is not the result of experimental uncertainty. Durning and coworkers studied sorption of methanol in annealed, semicrystalline PET by dipping it in liquid methanol ($p/p_o = 1$) at various temperatures [5]. They also observe an induction time followed by uptake that is linear with square root of time in the temperature range of 35–62 °C. However, they ignore the induction time, which is the fingerprint of non-Fickian effects, as an artifact because of the dominantly Fickian nature of the kinetics [6]. Hopfenberg and coworkers, and Windle and Thomas observed an induction time in the PMMA-n-propyl alcohol and PMMA-methanol systems respectively [46,47]. However, once mass uptake starts, the kinetics are clearly Case II as it is linear in time ($n = 1$ in equation 13). At higher temperatures, they observed that the features of anomalous kinetics appeared and approached Fickian behavior ($1/2 \leq n < 1$) [47,48]. The induction time also disappeared in these cases. There are no reports of the uptake kinetics showing Fickian features together with an induction time. The present observations of anomalous kinetics up to $p/p_o = 0.70$, coupled with an induction time, suggest that the amorphous PET at $p/p_o = 0.80$ and above most likely undergoes significant relaxations. An alternate way of looking at the kinetics would be to recognize the presence of an inflection point in the M_t/M_∞ plots at, approximately, 1.2 min. Crank notes that an inflection point can never occur in a completely Fickian curve [41]. Hopfenberg and Peterlin have observed such kinetics and show that this is predominantly relaxation driven [49,50]. Both the analyses seem to suggest that relaxation effects are involved here.

To confirm this, completely amorphous films of different thicknesses should be studied. Such samples with consistent preparation histories, however, were not available to us. It appears that there are relaxation/swelling effects involved; however the presence of Fickian behavior is difficult to explain without more data. The definitive test of Fickian characteristics is the collapse of all kinetics on to a master curve when plotted against $\sqrt{t}/l$. In PET–methanol case, there is a strong possibility that the relaxation and Fickian components will be separable when the characteristic dimensions are different. Moreover, the swelling of the sample and concentration dependent diffusion coefficients can be understood for this system.

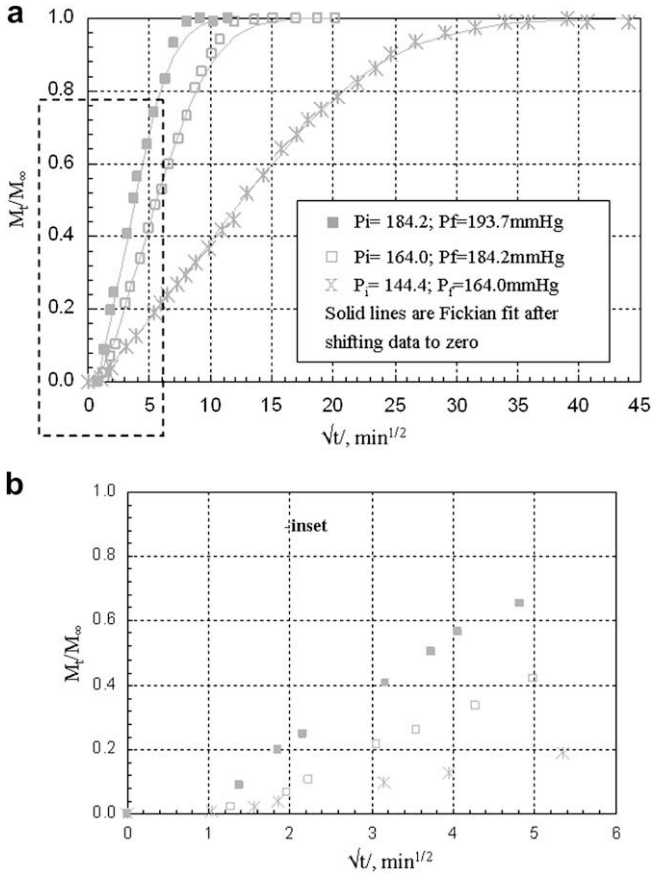

Fig. 11. (a) Kinetics of amorphous PET at high activities of methanol at 35 °C; (b) Inset showing the kinetics at small times with a clear induction time.

4. Conclusions

The results of this work support the following conclusions.

1. Sorption isotherms show dual mode characteristics at low activities of methanol at 35 °C, and Flory–Huggins features at high activities amorphous and semicrystalline, annealed samples. In the low activity regime, the diffusion coefficients followed concentration dependence predicted by the dual mode model. Permeability was predicted and model parameters evaluated.
2. Even at low methanol activities, hysteresis during desorption and increase in solubility during resorption suggest methanol induced conditioning effects. This conditioning may have detrimental effects on the barrier efficacy due to increased gas transport.
3. At high activities, significant relaxation and swelling effects are observed despite crystallinity and orientation. Such swelling may deteriorate the barrier properties of the polymer. Annealing effects reduce the relaxation effects, and coupled with lower solubility offer improved barrier efficacy than amorphous or non-annealed, oriented PET.
4. Unusual kinetics are observed in the amorphous film at high activities. It is hypothesized that these are strongly relaxation related and may be verified using films of different thicknesses.

Acknowledgements

The authors would like to acknowledge financial support from The Coca Cola Company for this research.

References

[1] Dhoot SN, Freeman BD, Stewart ME. Industrial and Engineering Chemistry Research 2004;43:2966–76.
[2] Patton CJ, Felder RM, Koros WJ. Journal of Applied Polymer Science 1984;29:1095–110.
[3] Dhoot SN, Freeman BD, Stewart ME. Polymer 2004;45:5619–28.
[4] Dhoot SN, Freeman BD, Stewart ME, Hill AJ. Journal of Polymer Science, Part B: Polymer Physics 2001;39:1160–72.
[5] Durning CJ, Rebenfeld L, Russel WB. Polymer Engineering and Science 1986;26:1066–78.
[6] Billovits GF, Durning CJ. Polymer 1988;29:1468–84.
[7] Escoubes M, Moser D, Berticat P. Angewandte Makromolekulare Chemie 1978;67:45–60.
[8] McBain JW, Bakr AM. Journal of the American Chemical Society 1926;48: 690–5.
[9] Koros WJ. Sorption and Transport in Glassy Polymers. University of Texas; 1977.
[10] Duabeny RdP. Proceedings of the Royal Society of London, Series A: Mathematical, Physical and Engineering Sciences 1954;226:531.
[11] Fakirov S, Fischer EW, Schmidt GF. Makromolekulare Chemie 1975;176:931.
[12] Lapersonne P, Bower DI, Ward IM. Polymer 1992;33:1266–76.
[13] Farrow G, Ward IM. Polymer 1960;1:330–9.
[14] Sharma V, Desai P, Abhiraman AS. Journal of Applied Polymer Science 1997;65:2603–12.
[15] Liu RYF, Hu YS, Schiraldi DA, Hiltner A, Baer E. Journal of Applied Polymer Science 2004;94:671–7.
[16] Bove L, D'Aniello C, Gorrasi G, Guadagno L, Vittoria V. Polymer 1996;37:5309–11.
[17] Lin J, Shenogin S, Nazarenko S. Polymer 2002;43:4733–43.
[18] Dlubek G, Sen Gupta A, Pionteck J, Haessler R, Krause-Rehberg R, Kaspar H, et al. Polymer 2005;46:6075–89.
[19] Koros WJ, Chan AH, Paul DR. Journal of Membrane Science 1977;2:165–90.
[20] Koros WJ, Madden W. In: Kroschwitz JI, editor. Encyclopedia of polymer science and engineering. 2nd ed., vol. supplement volume. New York: John Wiley; 1989.
[21] Gohil RM, Salem DR. Journal of Applied Polymer Science 1993;47:1989–98.
[22] Michaels AS, Bixler HJ. Journal of Polymer Science 1961;50:393–412.
[23] Slee JA, Orchard GAJ, Bower DI, Ward IM. Journal of Polymer Science, Part B: Polymer Physics 1989;27:71–83.
[24] Brolly JB, Bower DI, Ward IM. Journal of Polymer Science, Part B: Polymer Physics 1996;34:769–80.
[25] Vieth WR, Alcalay HH, Frabetti AJ. Journal of Applied Polymer Science 1964;8:2125–38.
[26] Berens AR. Journal of Applied Polymer Science 1989;37:901–13.
[27] Berens AR. ACS Symposium Series 1990;423:92–110.
[28] Flory PJ. Journal of Chemical Physics 1949;18:108–13.
[29] Zhou FB, Koros WJ. Polymer 2006;47:280–8.
[30] Wind JD, Sirard SM, Paul DR, Green PF, Johnston KP, Koros WJ. Macromolecules 2003;36:6442–8.
[31] Michaels AS. Journal of Applied Polymer Science 1963;34:13.
[32] Koros WJ, Paul DR. Journal of Polymer Science, Polymer Physics Edition 1978;16:1947–63.
[33] Jordan SM, Koros WJ. Journal of Membrane Science 1990;51:233–47.
[34] Jordan SM, Henson MA, Koros WJ. Journal of Membrane Science 1990;54: 103–18.
[35] Berens AR. Angewandte Makromolekulare Chemie 1975;47:97–110.
[36] Wonders AG, Paul DR. Journal of Membrane Science 1979;5:63–75.
[37] Al-Juaied M, Koros WJ. Journal of Membrane Science 2006;274:227–43.
[38] Connelly RW, McCoy NR, Koros WJ, Hopfenberg HB, Stewart ME. Journal of Applied Polymer Science 1987;34:703–19.
[39] Serad GE, Freeman BD, Stewart ME, Hill AJ. Polymer 2001;42:6929–43.
[40] Stewart ME, Hopfenberg HB, Koros WJ, McCoy NR. Journal of Applied Polymer Science 1987;34:721–35.
[41] Crank J. The mathematics of diffusion. 2nd ed. New York: Oxford University Press; 1975.
[42] Chandra P. Georgia Institute of Technology; 2006.
[43] McDowell CC, Freeman BD, McNeely GW. Polymer 1999;40:3487–99.
[44] Berens AR, Hopfenberg HB. Polymer 1978;19:489–96.
[45] Baird BR, Hopfenberg HB, Stannett V. Polymer Engineering and Science 1971;11:274.
[46] Hopfenberg HB, Nicolais L, Drioli E. Polymer 1976;17:195–8.
[47] Thomas N, Windle AH. Polymer 1978;19:255–65.
[48] Nicolais L, Drioli E, Hopfenberg HB, Caricati G. Journal of Membrane Science 1978;3:231–45.
[49] Hopfenberg HB. Journal of Membrane Science 1978;3:215–30.
[50] Peterlin A. Organic Coatings and Plastics Chemistry 1978;39:121–2.